

# At the extremes of nuclear charge and spin \*

W.D. MYERS AND W.J. ŚWIĄTECKI

Nuclear Science Division, Lawrence Berkeley Laboratory,  
Berkeley, California 94720

Using scaling rules valid in the liquid drop model of nuclei, as well as universal rules associated with exchanges of stability in families of equilibrium configurations, we constructed closed formulae in terms of the atomic and mass numbers  $Z$  and  $A$  and the angular momentum  $L$ , which represent the properties of nuclei rotating synchronously (with ‘rigid’ moments of inertia), as calculated numerically using the Thomas-Fermi model of [5,6]. The formulae are accurate in the range of mass numbers where the transition to rapidly elongating triaxial ‘Jacobi’ shapes takes place. An improved set of formulae is also provided, which takes account of the decreased moments of inertia at low angular momenta. The formulae should be useful in guiding experimental searches for the Jacobi transition. In the second part of the paper we discuss qualitatively some aspects of the dynamics of nucleus-nucleus fusion, and outline a possible way of estimating cross-sections for the synthesis of superheavy nuclei.

PACS numbers: 21.10.Dr, 21.60.Ev, 24.10.Nz

## 1. Introduction

In 1834 C.G.J. Jacobi made a startling discovery which led to the realization that, at a certain critical angular momentum, the stable equilibrium shape of a gravitating mass rotating synchronously (i.e., with all mass elements sharing a common angular velocity) changes abruptly from a slightly oblate spheroid to a triaxial ellipsoid rotating about its shortest axis [1]. In 1961 the suggestion was made in [2] that a similar phenomenon might be expected in the case of atomic nuclei idealized as charged incompressible liquid drops endowed with a surface tension. This was confirmed and quantified in 1974 [3] and 1986 [4]. In 1996 the oblate-to-triaxial transition

---

\* Presented by W.J. Świątecki at the XXXV Zakopane School of Physics, Zakopane, Poland, 5-13 September 2000. Proceedings to be published in Acta Physica Polonica.

was demonstrated also in the more realistic self-consistent, semi-classical nuclear Thomas-Fermi model under the same assumption of synchronous rotation [5]. The Thomas-Fermi model [6] provides a good description of shell-averaged static nuclear properties, but the assumption of synchronous rotation is known to be strongly violated at low angular momenta, where measured moments of inertia are considerably smaller than the ‘rigid-body’ values implied by synchronous rotation [7]. In the first part of the present paper we provide: a) closed formulae that represent accurately the energies and fission barriers of synchronously rotating Thomas-Fermi nuclei in the range of mass numbers where the Jacobi transition takes place, and b) modified formulae that take into account the decreased moments of inertia at low angular momenta.

In the second part (section 5) we present a discussion of some aspects of the dynamics of nucleus-nucleus fusion, and we sketch a possible way of estimating fusion cross-sections for the synthesis of heavy and superheavy nuclei.

## 2. Thomas-Fermi formulae

For each of the following six nuclei:  $^{74}\text{Se}$ ,  $^{94}\text{Mo}$ ,  $^{108}\text{Cd}$ ,  $^{126}\text{Xe}$ ,  $^{140}\text{Nd}$ ,  $^{168}\text{Yb}$ , we generated self-consistent stable as well as saddle-point solutions of rotating configurations using the Thomas-Fermi model of [5,6]. As a rule, the angular momenta ranged between  $L = 0$ , through  $L = L_1$ , where the Jacobi transition takes place, to  $L = L_2$ , where the barrier against fission of the Jacobi shapes vanishes. Using as a guide scaling rules valid in the liquid drop model (which is a lowest-order approximation to the Thomas-Fermi model [8]), as well as universal rules associated with bifurcations and limiting points in families of equilibrium shapes [9], we constructed formulae in terms of the atomic and mass numbers  $Z$  and  $A$  and the angular momentum  $L$ , which represent accurately the numerically calculated properties of the above six nuclei. These formulae, listed below, can then be used for neighbouring nuclei, thus avoiding the need for a separate Thomas-Fermi calculation for each additional nucleus of interest. In the following formulae all energies are in MeV, and angular momenta are in units of  $\hbar$ .

The critical angular momentum at which the Jacobi transition takes place:

$$L_1 = 0.06029A^{7/6}\sqrt{40.83 - \zeta}, \quad (1)$$

where the fissility  $\zeta$  is defined by

$$\zeta = Z^2 / A \left[ 1 - 1.7826 \left( \frac{A - 2Z}{A} \right)^2 \right]. \quad (2)$$

The angular momentum at which the fission barrier vanishes:

$$L_2 = 0.09108A^{7/6} \sqrt{36.34 - \zeta} . \quad (3)$$

The energy of the oblate (Maclaurin-like) equilibrium shapes (with respect to the non-rotating ground state):

$$E_M(L) = \gamma_1 L_1 \left( 0.3\lambda^2 - 0.025\lambda^4 \right) , \quad (4)$$

where

$$\gamma_1 = 6.2811 \sqrt{(44.60 - \zeta)/A} , \quad (5)$$

and

$$\lambda = L/L_1 . \quad (6)$$

The energy of the Jacobi shapes (for  $L_1 \leq L \leq L_2$ ):

$$E_J(L) = 0.275\gamma_1 L_1 + \frac{1}{2}\gamma_1 (L_2 - L_1) \left[ \Gamma_2(1 - X) + \frac{1}{2}(1 - \Gamma_2 - \beta)(1 - X^2) + \frac{2}{3}\beta(1 - X^{3/2}) \right] , \quad (7)$$

where

$$\Gamma_2 = 0.6118 \left[ 1 - (\zeta/38.91)^2 \right]^2 / \left[ 1 - (\zeta/33.49)^2 \right] , \quad (8)$$

$$X = (L_2 - L)/(L_2 - L_1) , \quad (9)$$

$$\beta = 0.3078 . \quad (10)$$

The energy of saddle-point shapes for  $L \leq L_2$  :

$$E_S(L) = 0.275\gamma_1 L_1 + \frac{1}{2}\gamma_1 (L_2 - L_1) \left[ \Gamma_2(1 - X) + \frac{1}{2}(1 - \Gamma_2 - \beta)(1 - X^2) + \frac{2}{3}\beta(1 + X^{3/2}) \right] . \quad (11)$$

The fission barrier for Jacobi shapes (with  $L_1 \leq L \leq L_2$ ):

$$B_J(L) = B_1 X^{3/2} , \quad (12)$$

where

$$B_1 = \frac{2}{3}\gamma_1\beta(L_2 - L_1) . \quad (13)$$

The fission barrier for Maclaurin shapes with  $L \leq L_1$ :

$$B_M(L) = \frac{1}{2}\gamma_1 (L_2 - L_1) \left[ \Gamma_2(1 - X) + \frac{1}{2}(1 - \Gamma_2 - \beta)(1 - X^2) + \frac{2}{3}\beta(1 + X^{3/2}) \right] - \gamma_1 L_1 (0.3\lambda^2 - 0.025\lambda^4 - 0.275) . \quad (14)$$

Now define energy derivatives by

$$\gamma(L) \equiv 2 dE(L)/dL , \quad (15)$$

so that

$$\gamma_L \equiv \gamma(L - 1) \quad (16)$$

is an accurate approximation to a nominal quadrupole transition energy from the state  $L$  to the state  $L - 2$ . Then for the Maclaurin shapes we have:

$$\gamma_M(L) = \gamma_1 [1.2\lambda - 0.2\lambda^3] \quad (17)$$

and for the Jacobi shapes with  $L_1 \leq L \leq L_2$  we find

$$\gamma_J(L) = \gamma_1 [\Gamma_2 + (1 - \Gamma_2 - \beta)X + \beta\sqrt{X}] . \quad (18)$$

For  $L = L_1$  we have  $\gamma_M(L_1) = \gamma_J(L_1) = \gamma_1$  . For  $L = L_2$  we have  $\gamma_J(L_2) = \gamma_1\Gamma_2$  .

The above equations are accurate representations of the numerical Thomas-Fermi solutions for mass numbers  $A$  greater than about 70 and less than about 170, or for fissilities  $\zeta$  greater than about 15.8 and less than about 30.7. They may also be adequate for  $A$  less than 70, but should not be used for  $A$  greater than about 170 (fissility greater than about 30.7). The expression for  $B_M(L)$  may not be reliable for  $L$  much below  $L_1$ .

Fig.1 compares the values of  $L_1$  and  $L_2$  with the liquid drop model values of [3] and with the finite range liquid drop model values of [4]. The curves for  $L_1$  up to  $A \approx 170$  are essentially the same in all three models. The Thomas-Fermi curve for  $L_2$  is usually intermediate between those of the other two models.

Fig.2 shows the energies  $E_M, E_J, E_S$  and the barrier  $B$  for the nucleus  $^{108}\text{Cd}$ .

Fig.3 shows the nominal quadrupole transition energies  $\gamma_L$  for  $^{94}\text{Mo}$ ,  $^{108}\text{Cd}$ ,  $^{140}\text{Nd}$  and  $^{168}\text{Yb}$ , the nuclei that would result after emission of four neutrons from the compound nuclei formed in the bombardments of  $^{50}\text{Ti}$ ,  $^{64}\text{Ni}$ ,  $^{96}\text{Zr}$  and  $^{124}\text{Sn}$  by  $^{48}\text{Ca}$ . These are the reactions recently studied in [10]. Fig.3 implies ‘giant backbends’ in the gamma ray energies  $\gamma_L$  at the critical values given by  $L = L_1 + 1$ , where the originally increasing gamma ray energies suddenly begin to decrease. This decrease is a hallmark of the Jacobi regime of shapes, associated with their rapidly increasing moments of inertia. (Note: eqs.(15,16) imply that if  $\gamma(L)$  has a maximum at  $L_1$ , then  $\gamma_L$  has a maximum at  $L_1 + 1$ .)

### 3. Modified formulae

Measured rotational spectra correspond to energies that, for low angular momenta, increase considerably faster than described by eq.(4) or illustrated in Fig. 2. The implied low effective moments of inertia are associated with nuclear pairing effects, and are expected to disappear at higher values of  $L$  [7]. In particular, in the regime of the very deformed Jacobi shapes rotating about the shortest axis, the energy estimated using moments of inertia associated with synchronous rotation ('rigid' moments of inertia) should be relatively accurate. We have accordingly modified the energy plots  $E(L)$  by interpolating between  $k$  times  $E_M(L)$ , Eq. (4), for small  $L$  (where  $k$  is a number greater than 1, which implies moments of inertia less than 1), and the formula for  $E_J(L)$ , Eq. (7), near  $L = L_2$ . Explicitly, the interpolation was done as follows:

$$E_{<} = \gamma_1 L_1 \left[ k \left( 0.3\lambda^2 - 0.025\lambda^4 \right) - a\lambda^n \right] \quad \text{for } L \leq L_1, \quad (19)$$

$$E_{>} = 0.275\gamma_1 L_1 + \frac{1}{2}\gamma_1 (L_2 - L_1) \left[ \Gamma_2(1 - X) + \frac{1}{2}(1 - \Gamma_2 - \beta)(1 - X^2) + \frac{2}{3}\beta(1 - X^{3/2}) + bX^2 \right] \quad \text{for } L_1 \leq L \leq L_2, \quad (20)$$

where, for a given  $k$ , the three quantities  $n, a, b$  are determined by the requirement of continuity of value, slope and curvature at  $L = L_1$ . The demand for continuity of the curvature is motivated by recognition of the fact that collective rotations about axially symmetric (Maclaurin-like) shapes do not take place in nuclei. This implies that, also at low angular momenta, collective nuclear rotations must take place about an axis that is not an axis of symmetry, for example about a minor axis of a prolate or triaxial shape. In that case the transition from such a shape to the rapidly elongating Jacobi-like shape does not involve a spontaneous oblate-to-triaxial symmetry breaking, and would be smooth rather than abrupt. The associated gamma ray energies would now be expected to change gradually from increasing to decreasing functions of  $L$ , which implies continuity of the second derivative of  $E(L)$ . (We shall continue to refer to the regime of decreasing gamma ray energies as the Jacobi regime.)

The abovementioned requirements of continuity lead to the following formulae for  $n, a, b$ :

$$n = \frac{-B + \sqrt{B^2 + 4AC}}{2A}, \quad (21)$$

$$a = \frac{A}{4 + 2n\kappa}, \quad (22)$$

$$b = \frac{1}{2}(1 - k + 2na), \quad (23)$$

where

$$A = (1.1 + \kappa)(k - 1) , \quad (24)$$

$$B = -A + \frac{A}{\kappa} - k(1 + 0.6\kappa) + \Gamma_2 + \frac{\beta}{2} , \quad (25)$$

$$C = \frac{2}{\kappa} \left( \frac{A}{\kappa} - A - B \right) , \quad (26)$$

where

$$\kappa = \frac{L_2}{L_1} - 1 . \quad (27)$$

Fig.4 illustrates the modified energies and fission barriers in the case of  $^{108}\text{Cd}$ . The value of  $k$  was taken to be 1.5 (see below).

The formulae for the energy derivative functions are now as follows:

$$\gamma_{<}(L) = \gamma_1 \left[ k \left( 1.2\lambda - 0.2\lambda^3 \right) - 2na\lambda^{n-1} \right] \quad \text{for } L \leq L_1 \quad (28)$$

$$\gamma_{>}(L) = \gamma_1 \left[ \Gamma_2 + (1 - \Gamma_2 - \beta) X + \beta\sqrt{X} - 2bX \right] \quad \text{for } L_1 \leq L \leq L_2 . \quad (29)$$

The Jacobi regime of decreasing values of  $\gamma(L)$  begins now at the giant back-bend angular momentum  $L_m$  (always less than  $L_1$ ) where  $\gamma_{<}(L)$  has its maximum. It is given by the solution of

$$k \left( 0.6 - 0.3\lambda_m^2 \right) - n(n-1)a\lambda_m^{n-2} = 0 , \quad (30)$$

where  $\lambda_m = L_m/L_1$ . (The maximum in  $\gamma_L$  is then at  $L_m + 1$  — see above.)

Varying  $k$  results in a one-parameter family of interpolation functions for  $\gamma_L$ , illustrated for  $^{94}\text{Mo}$  in Fig.5. The choice  $k=1.5$  leads to  $\gamma_L$  plots shown in Fig.6. This choice turned out to give a rough correspondence with the preliminary results of the measurements referred to earlier [10]. The original, unmodified curves in Fig.3 bear little resemblance to the data.

#### 4. Relation to microscopic calculations

In a recent preprint entitled “Very extended nuclear shapes near  $A=100$ ” R. R. Chasman describes a ‘cranked-Strutinsky’ study of 37 nuclei between  $^{100}\text{Zr}$  and  $^{122}\text{Xe}$ , at angular momenta  $L = 60$  and  $L = 70$  [11]. Many of these nuclei are found to have strongly deformed prolate or triaxial shapes, and to have fission barriers in the range from about 4 MeV to about 17 MeV. The circles in Fig.4 show these barriers in the case of  $^{108}\text{Cd}$ . For a sample of 17 out of the 37 cases studied by Chasman the deviations between the microscopic cranked-Strutinsky and the modified Thomas-Fermi barriers were  $-0.67 \pm 1.18$  MeV at  $L = 60$ , and  $0.41 \pm 1.53$  MeV at  $L = 70$ . (The

deviation for all 34 values at both  $L = 60$  and  $L = 70$  was  $-0.13 \pm 1.45$  MeV.) It is interesting to note that, since the Thomas-Fermi energies are smooth functions of  $A$ ,  $Z$  and  $L$ , one concludes that the microscopic energies are also smooth to within about 1.5 MeV on the average (or else that the shell corrections for the equilibrium shape and for the saddle-point shape are approximately the same). Also, considering the very different inputs in the two types of calculation, it is remarkable that, on the average, the absolute values of the fission barriers agree to within a fraction of an MeV. On the whole, one is led to the conclusion that Chasman’s “very extended shapes” and the Thomas-Fermi Jacobi configurations are the microscopic and macroscopic descriptions of the same underlying physics that goes back to 1834, namely: “Sufficiently rapidly rotating fluids prefer elongated prolate shapes”.

## 5. Fusion dynamics

It is an elementary everyday observation that if two fluid drops are brought into contact, there takes place a sudden growth of the neck — a snap — characterized by a time scale much shorter than those typical of other collective degrees of freedom of the system, such as its overall length. The driving force for this snap is the great saving of surface energy achieved with only a minor rearrangement of the fluid’s mass elements in the vicinity of the neck. Thus, insofar as nuclei can be regarded as fluids (see below for exceptions) the dinuclear configuration of touching fragments is expected to be transformed rapidly into a mononuclear shape with about the original overall length (which we shall refer to as the snap length). With reference to the potential energy landscape underlying the fusion process, the system, originally in the fusion valley, is injected into the vicinity of the fission valley at a point along this valley specified approximately by the snap length.

Once in the fission valley, the system may find itself either inside or outside the saddle-point barrier guarding the compound nucleus against disintegration by fission. For lighter reacting systems the former is the case and, after contact, fusion takes place automatically. But with increasing sizes of the reacting nuclei the saddle-point length shrinks rapidly, so that, beyond a certain critical point, the situation is reversed: after the snap the system is outside the saddle. The heavier the fusing partners the farther away from the saddle will the system find itself, and the greater will be the energy difference  $\Delta$  between the saddle-point energy and the system’s potential energy after injection into the fission valley. This is the physics of the entrance channel hindrance to fusion discussed in [12]. This hindrance may well be the principal reason for the rapid decrease of measured cross-sections for the formation of very heavy elements.

A second factor, *which acts in the opposite direction*, is present in the case of reactions at bombarding energies designed to leave the compound nucleus with a given excitation energy, for example the 13 MeV in the case of the reactions illustrated in Fig.7. As can be seen from this figure, the typical Coulomb barrier in the entrance channel would prevent the relatively lighter projectiles up to  $^{70}\text{Zn}$  from even achieving contact between the half-density nuclear surfaces. The implied hindrance, as represented by the size of the Coulomb barrier that protrudes above the level of the bombarding energy, is most pronounced for the lightest projectiles, decreasing with projectile size, and eventually disappearing altogether for the reaction  $^{86}\text{Kr} = ^{208}\text{Pb}$ . This lowering of the ‘Coulomb shield’ for superheavy reactions [13,14] is an elementary consequence of the energetics of nuclear deformations. Thus, the energy needed to deform a compound nucleus into the Coulomb barrier configuration of two touching fragments is resisted by the surface energy and favoured by the electrostatic energy. Hence, for a sufficiently large charge on the system, the Coulomb barrier will eventually sink below the level of the ground-state energy (or this energy augmented by some constant, like the 13 MeV in the examples above). This is illustrated in Fig.8.

Coming back to Fig.7, the hindrance against achieving contact would be 100% up to about  $^{70}\text{Zn}$ , and zero afterwards, if a classical, one-dimensional calculation were used. In a more realistic treatment, the hindrance would decrease gradually, and a quantitative description of such ‘sub-barrier’ fusion probabilities has been available for some time in terms of the notion of barrier height distributions [15].

Working together with K. Siwek-Wilczyńska and J. Wilczyński, we have been led by the above considerations to the following three-stage picture of the fusion process of heavy nuclear systems:

Stage 1: Overcoming the Coulomb barrier in order to achieve contact. Using existing theories of sub-barrier fusion, the relevant probabilities can be estimated. After contact, a snap from the fusion valley into the fission valley follows. The associated drop in the potential energy is assumed to heat up the system to a temperature  $T$ .

Stage 2: Overcoming the energy barrier  $\Delta$  necessary to reach the compound nucleus from the fission valley after the snap. We assume that this is achieved by a thermal fluctuation with a probability approximated by  $\exp(-\Delta/T)$ .

Stage 3: Surviving the competition between fission and neutron emission. Standard formulae for the relevant probabilities are again available.

With the above factors depending in different ways on the reaction parameters, there is no particular reason to expect the plot of the logarithms of the formation cross-sections in Fig.7 to continue as a linear function of the atomic number beyond  $Z = 112$ . In this connection it is interesting



to note that the empirical data in Fig.7 up to  $Z = 112$ , rather than being fitted by a straight line, may equally well be represented by a cubic that is made to pass through the point for  $^{86}\text{Kr} + ^{208}\text{Pb}$ , as shown in Fig.9.

A word about the assumption of a snap at contact, characteristic of fluids. Nuclei often do exhibit fluid properties, but exceptions occur when sufficiently strong magic or doubly magic shell effects may endow a nucleus with properties of an elastic solid [16]. In that case the snap may not occur at contact, but only after a more intimate interpenetration of the partners, sufficient to destroy their shell effects. Such a delay in the injection into the fission valley may be advantageous, since the resulting mononucleus will be more compact, and thus closer to the saddle-point configuration. (See the discussion in [13,14].)

We hope to develop the above qualitative considerations into a semi-empirical method of estimating cross-sections for the synthesis of heavy elements.

We would like to thank D.Ward, R.Diamond, F.Stephens, and P.Fallon for sharing with us information on the experimental searches for the Jacobi transition, and J.Wilczyński and K. Siwek-Wilczyńska for discussions of formation cross-sections for heavy nuclei. This work was supported in part by the Director, Office of Energy Research, Office of High Energy and Nuclear Physics, and by the Office of Basic Energy Sciences, Division of Nuclear Sciences, of the U.S. Department of Energy under Contract No. DE-AC03-76SF00098, and by the Polish-American Maria Skłodowska-Curie Fund No. PAA/NSF-96-253.

## REFERENCES

- [1] See S.Chandrasekhar, *Ellipsoidal Figures of Equilibrium*, Yale University Press, New Haven and London, 1969.
- [2] R.Berlinger and W.J.Knox, Phys.Rev. **121**, 1195(1961).
- [3] S.Cohen, F.Plasil and W.J.Swiatecki, Ann.Phys.(N.Y.) **82**, 557(1974).
- [4] A.J.Sierk, Phys.Rev.**C33**, 2039(1986).
- [5] W.D.Myers and W.J.Swiatecki, Acta Physica Polonica **27A**, 99(1996); Nucl.Phys. **A612**, 249(1997).
- [6] W.D.Myers and W.J.Swiatecki, Nucl.Phys. **A601**, 141(1996).
- [7] A.Bohr and B.Mottelson, *Nuclear Structure*, Benjamin, N.Y. 1975; Table of Isotopes, 8th edition, ed. R.B.Firestone and V.S.Shirley, Wiley, N.Y. 1996; W.D.Myers and W.J.Swiatecki, Nucl.Phys. **A641**, 203(1998), especially Figs.4-9.

- [8] W.D.Myers and W.J.Swiatecki, Ann.Phys. (N.Y.) **55**, 395(1969); **84**, 186(1974); W.J.Swiatecki, Nucl.Phys. **A574**, 233c(1994).
- [9] A general discussion of the ‘exchange of stability’ between families of equilibrium shapes goes back to H.Poincaré, as described in P.Appell, *Traité de Mécanique Rationnelle*, Gauthier-Villars, Paris 1932. See also R.Thom, *Parabole et Catastrophe*, Flammarion, 1983. In the case of two families that cross in a ‘pitchfork’ pattern, the energy difference between them grows as the second power of the distance from the crossing; in the case of a linear crossing, it is the third power; in the case of a ‘limiting point’ it is the three-halves power. For some relevant examples see W.J.Swiatecki, Phys.Rev. **101**, 651(1956).
- [10] D.Ward et al., in preparation.
- [11] R.R.Chasman, “Very Extended Nuclear Shapes Near A=100”, Argonne National Laboratory Physics Division preprint PHY-9018-Th-98.
- [12] J.B.Blocki, H.Feldmeier and W.J.Swiatecki, Nucl.Phys. **A459**, 145(1986) and references therein.
- [13] W.D.Myers and W.J.Swiatecki, Acta Physica Polonica **B31**, 1471(2000).
- [14] W.D.Myers and W.J.Swiatecki, Phys.Rev. **C62**, 044610(2000).
- [15] N.Rowley, G.R.Satchler and P.H.Stelson, Phys.Lett. **B254**, 25(1991) and, for example, J.D.Bierman et al., Phys.Rev. **C54**, 3068(1996).
- [16] J.Blocki, J.Skalski and W.J.Swiatecki, Nucl.Phys. **A594**, 137(1995); **A618**,1(1997) and references therein; W.J.Swiatecki, Nucl.Phys.**A488**, 375c(1988).

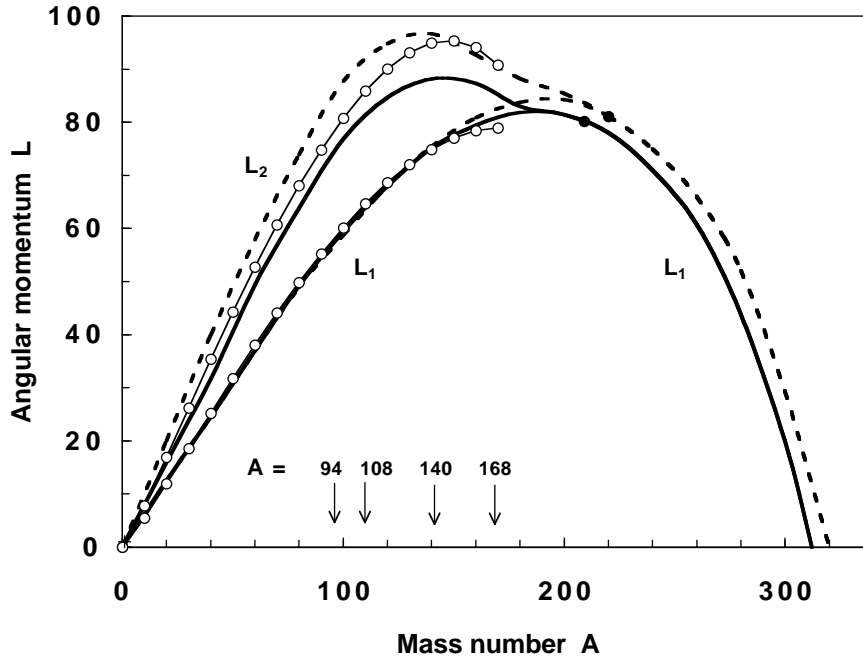


Fig.1. For angular momenta below the curves labeled  $L_1$  the equilibrium shape is an oblate configuration rotating about its axis of symmetry. The three models in question are identified by the dashed, solid and circled curves, representing the liquid drop model of [3], the finite range liquid drop model of [4] and the present Thomas-Fermi model, respectively. Between  $L_1$  and  $L_2$  the equilibrium shapes are triaxial Jacobi configurations rotating about the shortest axis. The curves  $L_1$  and  $L_2$  come together at the solid circles, beyond which mass numbers Jacobi shapes do not exist. Disintegration takes place for angular momenta exceeding  $L_1$  in the upper range of mass numbers, or  $L_2$  below the solid circles. The curves refer to nuclei on the valley of beta stability. The four arrows identify approximately the mass numbers of nuclei studied in [10].

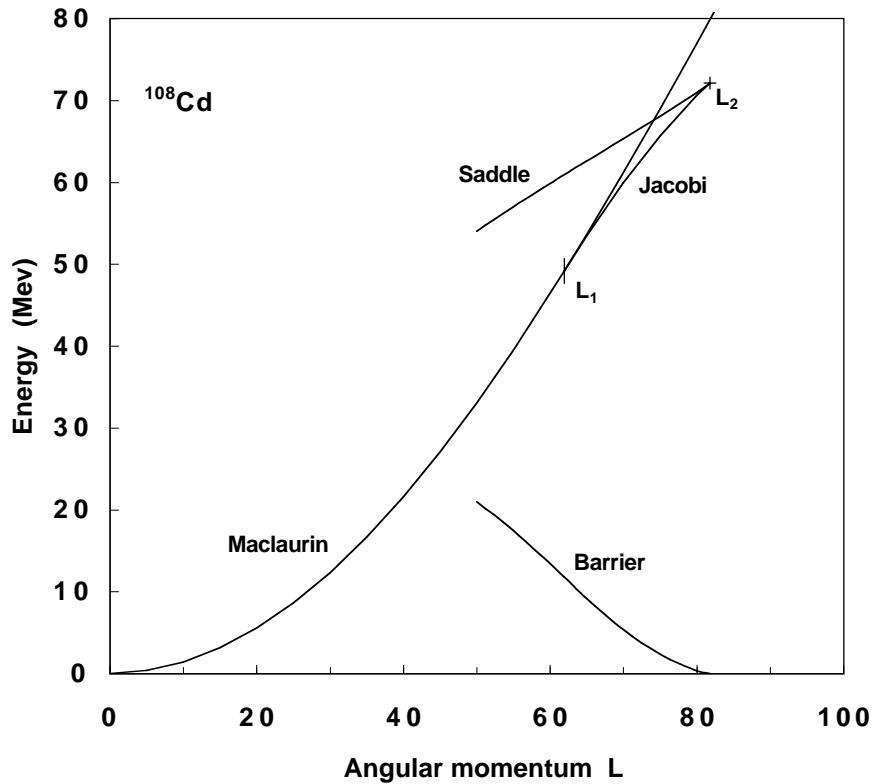


Fig. 2. The energies of the Maclaurin-like oblate shapes, the Jacobi-like triaxial shapes and the (triaxial) saddle-point shapes are shown in their dependence on angular momentum for  $^{108}\text{Cd}$ . The Jacobi shapes first appear at  $L_1$  and exist up to  $L_2$ . The fission barrier  $B$  is the energy difference between the saddle energy and either the Jacobi energy for  $L \geq L_1$  or the Maclaurin energy for  $L \leq L_1$ . It vanishes at  $L_2$ .

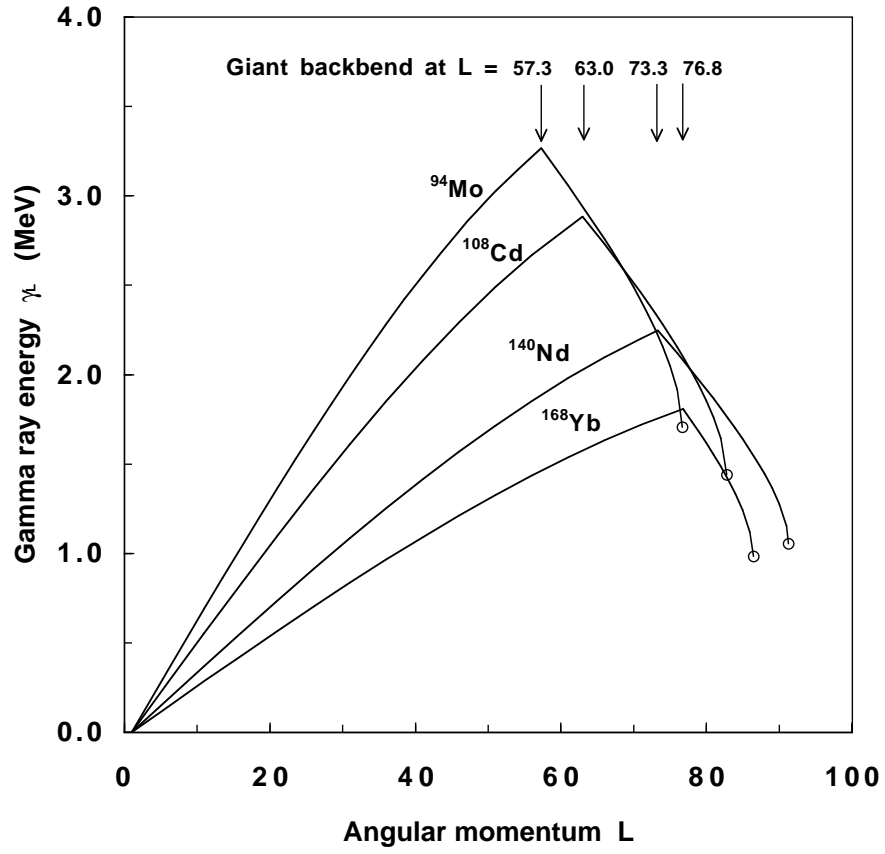


Fig. 3. The nominal quadrupole gamma ray energies  $\gamma_L$  are shown in their dependence on  $L$  for four nuclei. These curves represent the unmodified Thomas-Fermi model, with sharp giant backbends at the angular momenta indicated. The Jacobi shapes exist beyond the backbend and terminate at the circled points.

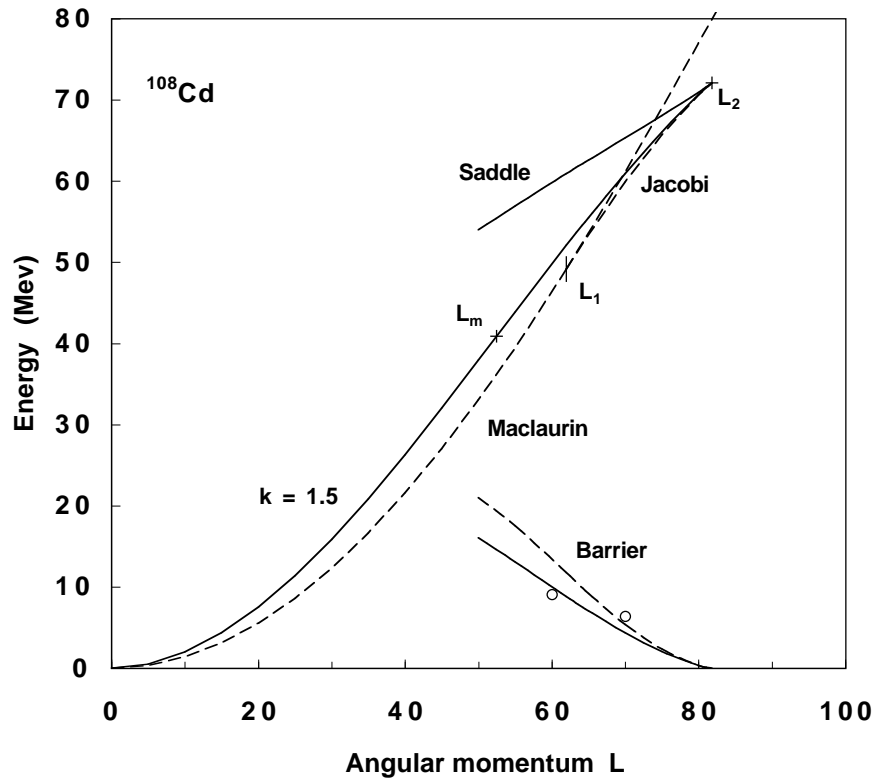


Fig. 4. The dashed curves repeat the plot from Fig.2, and the solid curves show the modification resulting from taking account of the reduction of the moment of inertia at low  $L$  by a factor of 1.5. The Jacobi regime of decreasing gamma ray energies begins now at the angular momentum  $L_m$ . The two circled points refer to fission barriers obtained with the cranked-Strutinsky method in [11].

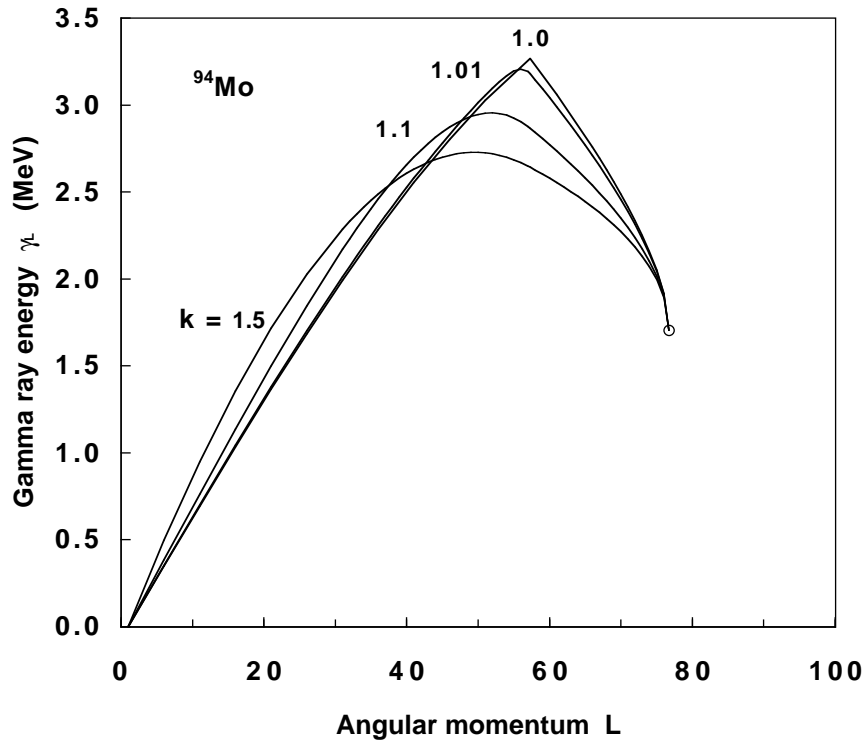


Fig. 5. The nominal quadrupole gamma ray energies for  $^{94}\text{Mo}$ , calculated using a modification of the Thomas-Fermi results, the modification consisting of assuming the low- $L$  moments of inertia to be reduced by 1.01, 1.1 and 1.5, respectively. The curve labeled 1.0 is the unmodified Thomas-Fermi result.

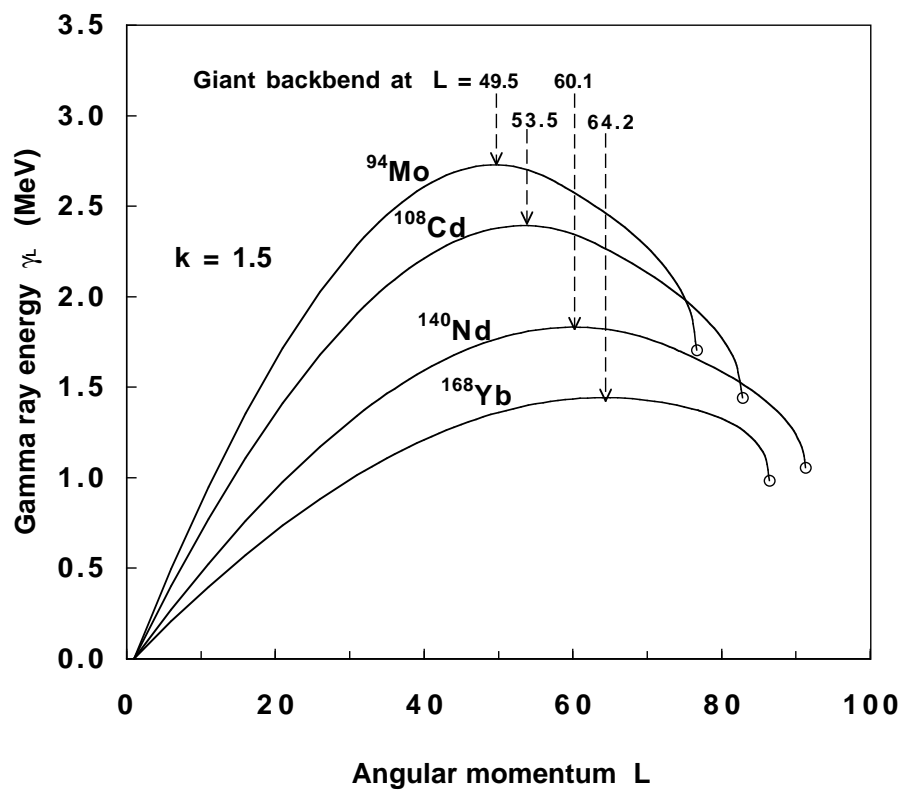


Fig. 6. This is like Fig.3, but after the modification consisting of reducing the low- $L$  moments of inertia by a factor 1.5. The giant backbends, marking the beginnings of the Jacobi regimes, are indicated by the arrows.



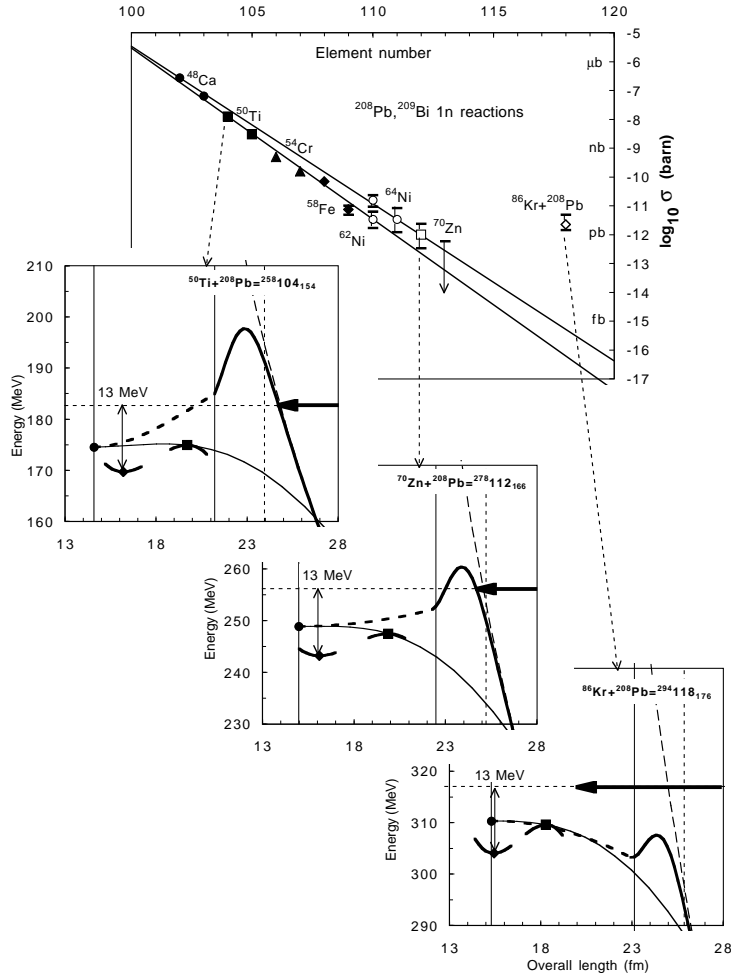


Fig. 7. The upper part refers to cross sections for synthesizing heavy elements from  $Z=102$  to  $118$  in bombardments of  $^{208}\text{Pb}$  and  $^{209}\text{Bi}$  with projectiles from  $^{48}\text{Ca}$  to  $^{86}\text{Kr}$ . The lower part gives three examples of (center-of-mass) potential energy plots along the fusion valley (thick solid and dashed curves) and fission valley (thin curves). The plots are against the overall, tip-to-tip extension of the fusing or fissioning configurations. The ground states are indicated by diamonds, the saddle-points by squares. The solid vertical line corresponds to contact between the half-density radii, the dashed vertical line to contact of the density tails, defined by the classical turning points of the fastest particles in the approaching nuclei. The horizontal arrow defines the bombarding energy, designed to leave the compound nucleus with 13 MeV of excitation energy.

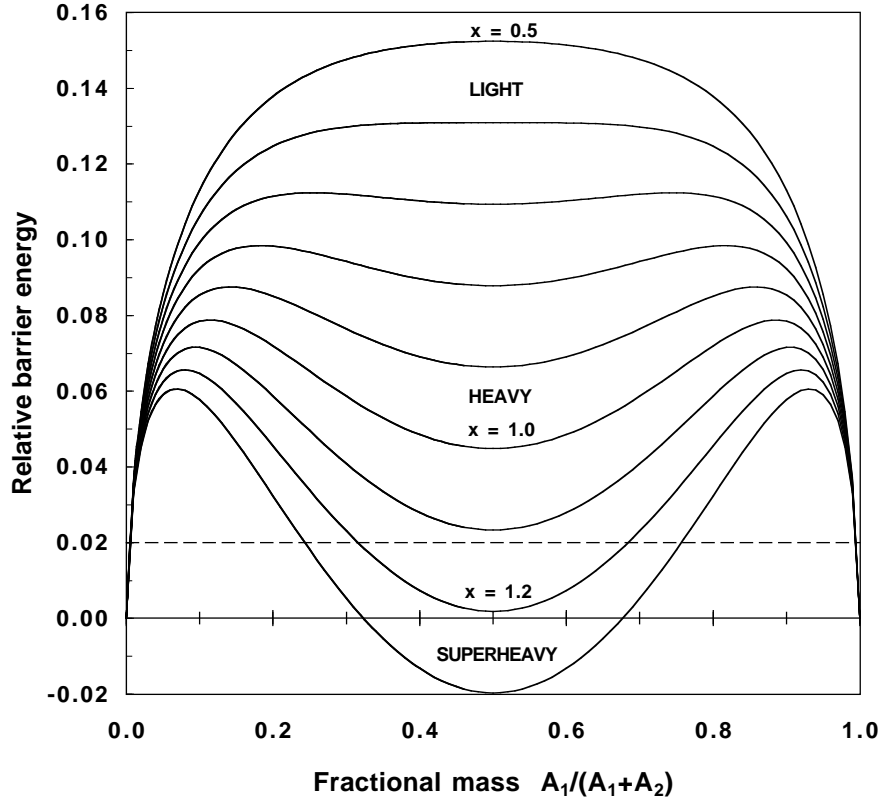


Fig. 8. This is the energy of tangent spheres (representing the Coulomb barrier) with respect to the energy of the single-sphere configuration (representing the compound nucleus), in units of that sphere's surface energy. The plots are against the asymmetry of the reaction. The label  $x$  is the standard fissility parameter, defined as the ratio of the electrostatic energy of the compound sphere to twice its surface energy. For  $x$  slightly in excess of 1.2 the Coulomb barrier (in this schematic liquid drop model) sinks below the energy of the compound nucleus. (This 'unshielding' would occur earlier with respect to a somewhat higher bombarding energy that would allow for the emission of one neutron. This is indicated schematically by the dashed line.) In either case the unshielding is characteristic only of extremely heavy (superheavy) systems and, as a rule, would not be expected to have been present in most heavy nucleus-nucleus reactions studied so far. (Quantitative aspects of this figure become modified when a more realistic macroscopic model is used, and when shell effects are taken into account.)

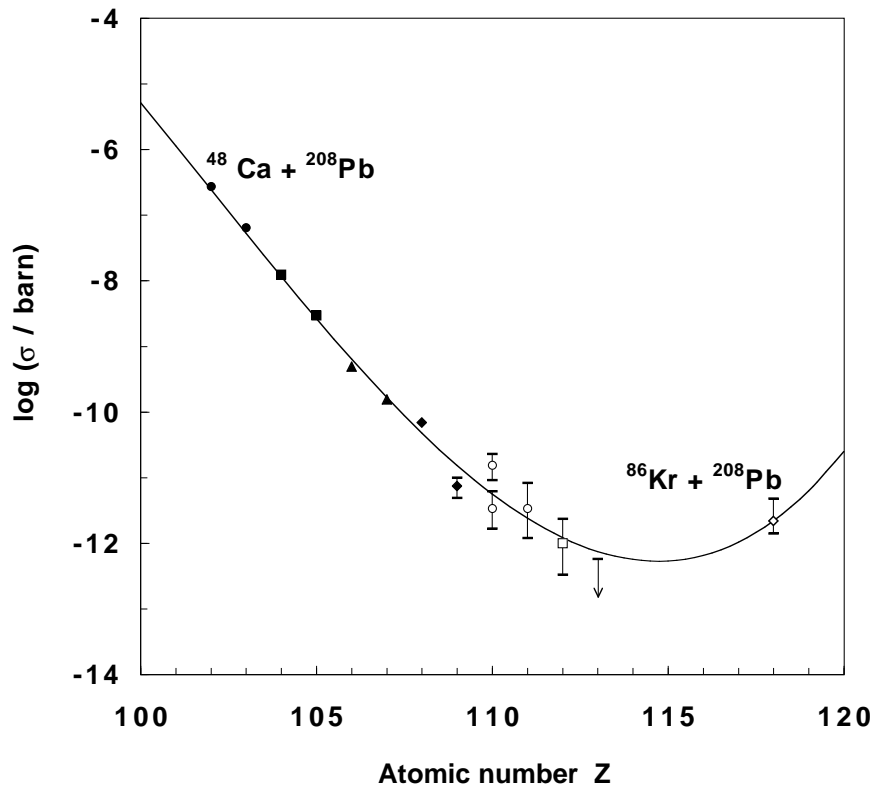


Fig. 9. The data points are the same as in the upper part of Fig.7. The curve is the cubic given by:  $\log(\sigma/\text{barn}) = -6.61 - 0.6681(Z - 102) + 0.001377(Z - 102)^3$ .